Collision of a Field-Driven Polymer with a Finite-Sized Obstacle: A Brownian Dynamics Simulation

P. M. Saville and E. M. Sevick*

Research School of Chemistry, The Australian National University, Canberra ACT 0200, Australia

Received July 2, 1998; Revised Manuscript Received November 2, 1998

ABSTRACT: We study the problem of a field-driven polymer chain of N monomers of size a colliding with a finite-sized obstacle of radius R in the presence of thermal noise. We show that there are two different mechanisms for chain release from the obstacle: "unhooking" and "rolling off". The unhooking mechanism is characterized by strong stretching of the chains at release and an unhooking time which scales with chain length. In contrast, the "rolling-off" mechanism does not impose strong stretching on the chain conformation and is dependent not upon the size of the chain, but rather upon the size of the obstacle. Thus, macroscopic mobility in an array of small, widely spaced posts provides an opportunity to separate chains according to their size, while chain mobility in an array of large circular obstacles provides information on the size of the obstacles. While important at small time scales, diffusion does not contribute significantly to the release kinetics from circular obstacles of any size R when the dimensionless field strength, defined as $\beta = E\lambda a/(k_B T)$ where λ is charge density and E is field strength, is $\beta N > a/R$.

I. Introduction

The dynamics of polymers is a well-developed field of study.[1] However, there are still several problems of fundamental importance which have not been fully explored. Surprisingly, many of these are in the area of single chain dynamics. Interest in single chain problems has been spurred in recent years by the advent of new experimental techniques that allow one to see and to manipulate individual polymer chains.[2−4] The particular problem presented in this paper is the collision of a field-driven polymer with a fixed obstacle. This problem has application in the size separation of polyelectrolytes of the same charge density, such as DNA, using electrophoresis. In electrophoresis, charged chains are driven through an array of obstacles by an applied electric field of magnitude E. These obstacles, usually gel fibers, impede the chain dynamics in a way that depends on the degree of polymerization, N, or size of the chain. The premise is that the degree to which the chains are "held up" by the obstacle imparts size dependence to the chain mobility, and in this way microlithographic arrays of posts might be exploited to enhance size separation.[5−7] If chains have differing charge densities, as in proteins, then separation occurs both in molecular size and in molecular charge. A description of the dynamics of a chain near an obstacle is also important in other applications, such as the flow of a dilute solution of chains through finely divided porous media. Apart from this application to electrophoresis, the interaction of a chain with an obstacle is a fundamental problem in polymer science which is analogous to the Rutherford scattering problem in atomic physics.

The effect of a small, frictionless obstacle upon the dynamics of field-driven chains is demonstrated simply by snapshots which were computer-generated using the simulation described in this paper. Figure 1 shows long and short chains at equivalent time steps. Note that those chains which do not impact upon the fixed obstacle advance downfield at a size-independent rate. The chains that impact directly upon the obstacle undergo dramatic conformational change, forming long-lived hairpins. The unraveling of a hairpin requires that one arm retract against the field, feeding the advancing arm. The rate of this unraveling is determined, in part, by the length or degree of polymerization, N, of the chain. Upon "release", the center of mass of the smaller hairpin has advanced downfield of the larger hairpin, and further advance occurs at a size-indpendent rate while the chain conformation relaxes. As a result of multiple collisions, larger chains will have a lower mobility than smaller chains, and consequently, size separation is possible. Although the unraveling of a hairpin, pictured in Figure 1, can be rate determining, most chains do not form hairpins about the obstacle.[8−11] Usually, chains do not impact the obstacle directly; impacts may range from glancing to head on, each with a different release

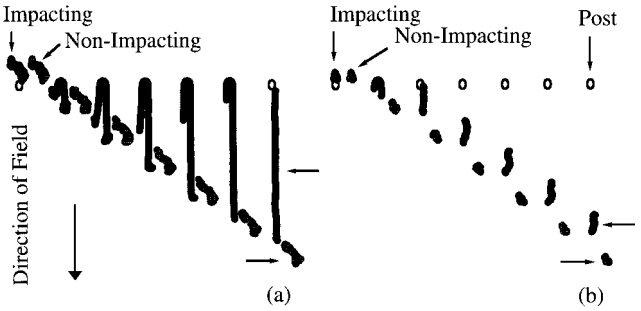

Figure 1. Snapshots of simulated chains interacting with a fixed obstacle at fixed time intervals and under high field strength, $E = 20$. Chains that do not collide with the obstacle are observed to travel downfield at constant velocity, irrespective of chain length. On the other hand, chains that directly impact the obstacle form hairpins and advance downfield at a hindered rate. The large, interacting chain (a) is suspended on the obstacle over a longer time than the shorter interacting chain (b). The arrows point to the centers of mass of the chains at the last time interval. The center of mass of the large interacting chain has not advanced downfield to the extent of that of the smaller, interacting chain. Hence, the interaction with the obstacle has imparted size dependence to the chain's mobility. Beyond this last time interval, the chain conformations relax, and the center of mass of all chains advances downfield at the same rate.

* Corresponding author.

10.1021/ma981049g CCC: $18.00
Published on Web 01/14/1999

trajectory. When hairpins do form, they may be multiple hairpins with smaller release times, or they may be partial hairpins which quickly slide off of the obstacle. A deterministic model that used a wide range of impact conditions from head-on to glancing, showed that perfect hairpin unhooking was rare in high fields with point, frictionless obstacles.[11] However, despite the wide variety of release trajectories found, the dynamic data follow universal curves over a large range of chain lengths and strong field strengths. These universal curves are important in that they suggest obstacle spacings for optimal size separation of polyelectrolytes; however, they are limited to point obstacles with no thermal noise.[11]

Most of the previous studies of polymer/single-obstacle collisions have tended to focus on small or pointlike obstacles or have used deterministic models of chain motion.[7,11−15] While such studies represent a good starting point for research, they do not include simultaneously two important and practical effects, namely obstacle size and thermal noise. Obstacles will often have a finite size. For example, λ-DNA with 48.6 kbp and 20 μm contour length has natural dimensions of $\approx$0.5 μm, which is comparable with a 1 μm post-obstacle fabricated using conventional microlithography. In high field with small obstacles, thermal noise can be safely ignored, and a deterministic description can be used. However, as the field is lowered or the obstacle size is increased, thermal noise plays an increasing role in the chain dynamics. In addition, an obstacle of appreciable size distorts the local electric field, although it is possible to fabricate ionically conducting obstacles out of agar gel.

In this paper we use a Brownian dynamics simulation to investigate the effect of obstacle size upon the collision time and distance moved during collision. We focus solely upon the interaction of a chain with a single obstacle, and we do not consider chain interaction with multiple obstacles. These quantities are crucial to determining the overall mobility of a chain in an array of obstacles and, hence, the ability of the obstacles to size-separate charged chains. We demonstrate that there are two modes of release which result from different obstacle sizes and field strengths. The first release mode consists of "unhooking" of a chain which is draped over the obstacle and is characterized by dramatic chain stretching during the collision. We find that this "unhooking" mechanism is operative for small posts and high fields and is characterized by universal scaling relations which suggest size separation capabilities.[11] The second release mode consists of a chain "rolling off" of the obstacle with little conformational change. Obstacles that are large in comparison to the chain size give rise to this rolling-off mechanism. Unlike unhooking, the characteristic time of rolling off is independent of chain length. Consequently, such roll-off collisions do not impart size dependence to the overall mobility of the chains. Indeed, the roll-off time is sensitive to the impacts, i.e., whether the chain impact is direct or glancing, and therefore roll-off collisions reduce resolution in size separation applications.

The remainder of the paper is organized in the following manner. In the next section we describe the simulation method that is used to follow the dynamics of two-dimensional Gaussian chains impacted against circular obstacles in constant and uniform electric fields. Individual chain trajectories which signature unhooking and rolling are investigated and characteristic times for the different modes of release are discussed in section III. In section IV we focus upon the collision of a chain against a large obstacle allowing for a range of impacts, varying from glancing to direct, and in section V we investigate an ensemble of chains colliding with obstacles of different sizes and in different field strengths. We show that the unhooking and rolling mechanisms can be separated and that chains which unhook follow universal scaling laws. In the final section we summarize our results with implications for size separation.

II. Simulation of the Dynamics of Chain Impact upon Obstacles

In a Langevin simulation, we are interested in time and lengths scales for which inertial effects become negligible; i.e., Newton's law of motion, $\mathbf{F} = m\mathbf{a}$, becomes effectively $\mathbf{F} = \mathbf{0}$. Thus, the simulation solves for the chain displacement which occurs when the sum of forces acting along points in the chain contour is set to zero. A deterministic force, $\mathbf{F}_{\mathrm{det}}$, is balanced by a drag force, $-\xi\mathbf{v}$, where ξ and $\mathbf{v}$ are the drag coefficient and velocity, and the displacement is $\Delta\mathbf{r} = \Delta t\xi^{-1}\mathbf{F}_{\mathrm{det}}$. The force of the surrounding solvent, represented by random forces, modifies this. The random forces are characterized by a Gaussian distribution with zero mean and variance $2\xi k_{\mathrm{B}}T$ where $k_{\mathrm{B}}T$ is the thermal energy. The displacement due to the random noise scales as $\Delta t^{1/2}$, and the total displacement is

$$\mathbf{r}(t + \Delta t) = \mathbf{r}(t) + \xi^{-1}\mathbf{F}_{\mathrm{det}}\Delta t + (2k_{\mathrm{B}}T\xi^{-1})^{1/2}\mathbf{g}(t)\sqrt{\Delta t}$$

where $\mathbf{g}(t)$ is a vector of Gaussian random numbers with zero mean and unit variance. The simulations in this paper are completed in two dimensions, i.e., $\Delta\mathbf{r} = \Delta y\mathbf{e}_y + \Delta z\mathbf{e}_z$ where $\mathbf{e}_y$ and $\mathbf{e}_z$ are unit vectors perpendicular and parallel to the applied field, respectively.

The dynamics of a polyelectrolyte is given by this equation applied to points along the contour of the chain. As our aims deal with molecular rather than atomic length/time scales, the chain contour is taken as a series of N beads connected by Hookean springs. The charge is localized at the beads, which serve as points over which the local forces balance. The deterministic force, $\mathbf{F}_{\mathrm{det}}$ is comprised of the electric force, $\lambda\mathbf{E}$ where λ is the charge per bead. We have assumed that the electric field is everywhere uniform, including near the obstacle; i.e., the obstacle is assumed to be ionically conductive and does not locally distort the electric field. Another component of $\mathbf{F}_{\mathrm{det}}$ is the spring force, $2k_{\mathrm{s}}(\Delta\mathbf{l}^{-} + \Delta\mathbf{l}^{+})$ where $\Delta\mathbf{l}^{\pm}$ are the extensions of the adjacent springs outside a natural length $a = 1$ and k_{s} is a spring constant. Also included in $\mathbf{F}_{\mathrm{det}}$ are any repulsive forces attributed to volume-excluding obstacles. Beads are prohibited from intersecting the hard core obstacle of radius H by a soft repulsion zone surrounding the obstacle core (Figure 2). This repulsive force decreases linearly with slope k_{r} from the core surface to zero at a distance R from the core center. We have neglected a number of contributions to $\mathbf{F}_{\mathrm{det}}$ that arise from counterions, electroosmotic flows, and hydrodynamic interactions, as well as detailed potentials that distinguish specific polyelectrolytes or proteins. A description of the balance of hydrodynamic interactions of the monomers and ion cloud which exist during free electrophoresis can be found in other works ranging from early classical

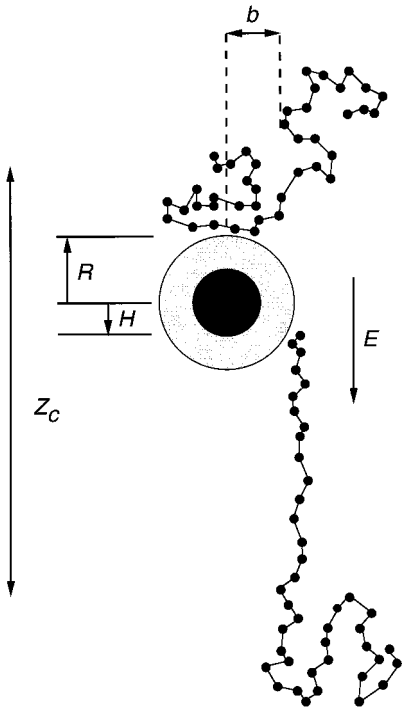

Figure 2. Schematic of the chain interacting with a fixed obstacle at time $t = 0$ and at the time of release, t_c, from the fixed obstacle. The obstacle has an inner hard core of radius H surrounded by a soft-repulsive zone extending to a distance R from the obstacle center at (0,0). The chain is modeled by N beads linked by extensible springs. The chain's center of mass is initially ($t = 0$) offset from the obstacle center by a lateral distance b, referred to as the impact parameter, and is upfield of the obstacle such that the most downfield bead is just touching the repulsive core of the obstacle. Release occurs when the last monomer has advanced past the hard core of the obstacle ($z = H$). The downfield advance of the center of mass and the time taken from initial to release are recorded as the collision distance, z_c, and collision time, t_c.

works to the most recent of studies.[16−18] However, as recently demonstrated, the inclusion of hydrodynamic interactions in the chain/obstacle problem has no significant effect on the overall collision time or the extent of chain stretching in strong fields.[18] In light of this result and of the complexity of a proper hydrodynamic treatment, hydrodynamics are not included in this study. The time step, Δt, and the force constants, k_s and k_r, are chosen such that the beads, their displacement vectors, and the connecting springs do not intersect the hard core of the obstacle.

The starting chain is created as a random, freely jointed chain of links, whose lengths are chosen from a Gaussian distribution. The natural size of the relaxed chain is characterized by its squared radius of gyration, $Na^2/6$. The linear extent, $\langle l \rangle$, is the average maximum separation of beads within the chain. The chain is located at a position upfield of the obstacle with its center of mass at ($\pm b$,z) relative to the obstacle center at (0,0) (Figure 2). The lateral displacement, b, of the chain is referred to as the impact parameter. Small b, i.e., $b \approx 0$, is indicative of direct impacts while large b, i.e., $b > R$, describes chain impacts that will only glance the obstacle. The initial z-location of the center of mass is selected such that the most downfield bead is located at $z = -R$. We define a dimensionless field strength as $\beta = E\lambda a/k_B T$ and characterize large fields as those where $\beta N \gg 1.0$ and weak field as $\beta N \ll 1.0$. The above equation is solved for the positions of each of the N beads over consecutive time steps. The time taken for all beads to have trespassed beyond $z = H$ is recorded as the collision time, t_c. The downfield distance that the chain's center of mass has traveled during t_c is recorded as the collision distance, z_c.

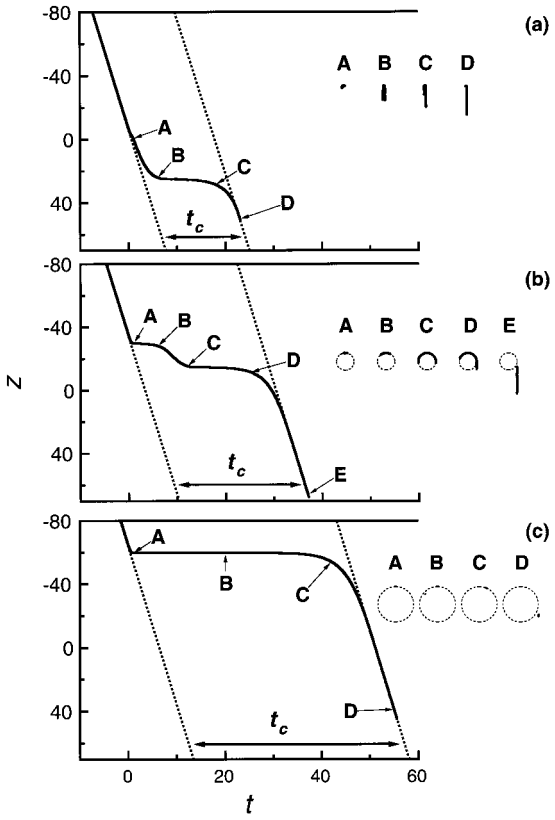

Figure 3. Downfield advance, $z_c(t)$, of the center of mass of $N = 100$ chains impacting directly upon obstacles of various sizes (a) $R = 3$ or $\gamma = 0.74$, (b) $R = 30$ or $\gamma = 7.4$, and (c) $R = 60$ or $\gamma = 15$. The dotted lines show the center of mass advance of chains that are unimpeded by obstacles. In (a) the impacted chain forms a hook around the small obstacle, $\gamma = 0.74$, and the retarded advance of the center of mass is attributed to unhooking of the chain. In (b) the impacted chain forms a hook, although the time required to form the hook over the larger obstacle $\gamma = 7.4$ is on the order of the unhooking time. In (c) the impacted chain rolls off of the large obstacle, $\gamma = 15$, without hook formation.

III. Trajectories of Chains Impacted Directly upon Obstacles of Different Size

Using the simulation, it is possible to follow the trajectory of the chain as it impacts the obstacle, is slowed by the obstacle, and then is finally released. It is convenient to represent this trajectory by the downfield advance of the chain's center of mass, $z_c(t)$, and to characterize the obstacle size by the ratio of the obstacle radius to the radius of gyration of the chain, $\gamma = R/(a\sqrt{N/6})$. In the absence of obstacles the downfield velocity of the center of mass is $v_0 = dz/dt = E\lambda/(a\xi)$. Prior to impact and after release, all chains will advance at this constant velocity. However, during collision, the chain will advance downfield at a slower rate within the range $0 < dz_c/dt < v_0$. Figure 3 shows the downfield advance of chains that impact directly ($b = 0$) on an obstacle with size $\gamma = 0.74$, 7.4, and 15. The dotted lines provide the unimpeded advance in the absence of the obstacles, and the lateral displacement of these lines is the time of the collision, t_c. The time of collision of the

three trajectories shown increases with the size of the obstacle. For the smallest obstacle, the chain's downfield center of mass velocity changes continuously throughout the collision, slowing toward the midpoint in the collision and increasing afterward toward release. The plateau in the downfield displacement−time curve corresponds to the slow unhooking process. When the obstacle is increased 10-fold in size, hooking still occurs in many trajectories. The particular chain trajectory shown in Figure 3b shows that the downfield advance of the chain is nearly halted immediately after impact with an additional plateau before release. This first plateau of near-zero advance is due to the significant size of the obstacle and reflects the time that it takes for portions of the chain to find the "edges" of the obstacle. Once found, the hook formation is rapid with a significant increase in the downfield velocity of the center of mass. The second plateau is due to the slow unhooking process. The unhooking process is slowed by the increased obstacle size. Simplistically, we can understand this as a result of the breadth of the hook: those monomers that reside at the flat top of the hook do not contribute significantly to the downfield tension in any of the arms of the hook. Consequently, as the obstacle increases in size, the arm lengths of the hook are shorter, the downfield tension on the chain is reduced, and the unhooking procedure is slower. When the obstacle is so large that the chain is unlikely to span the extent of the obstacle, release occurs as the monomers simply fall or roll off of the obstacle. In the particular chain trajectory of Figure 3c, the obstacle is much larger than the natural chain dimensions (γ = 15), chain hooking does not occur, and release occurs through the rolling off of monomers from the obstacle.

Simple deterministic models can be formulated for the unhooking of a chain from a point obstacle and for the rolling off of a chain from a large circular obstacle in strong fields. The characteristic time for unhooking can be obtained from a simple analysis of an inextensible chain with linear charge density λ, draped over the obstacle. The unhooking process is described by the increase in the difference in arm lengths, Δ. The time for unhooking in strong fields is found by equating the driving force for unhooking, $\Delta\lambda E$, with the drag force along the chain contour, $-\xi\, \mathrm{d}\Delta/\mathrm{d}t$ where $\xi = Na\eta$ and η is the viscosity. This characteristic time of unhooking, $t_{unhook} \approx a\eta/\lambda(N/E)$, is chain length-dependent. The second characteristic time scale of interest is that for chain roll-off from a large circular obstacle of radius R. The rolling-off process is described simply as the field-induced rolling of an object of charge $N\lambda$ along the path s on the obstacle surface. The drag on the object, $-\xi\, \mathrm{d}s/\mathrm{d}t$, is balanced by the component of the applied field force tangential to the obstacle surface, $\lambda NE \sin\theta$. The time that it takes for the object to roll from the near top of the obstacle to it side, $s = s_0$ to $s = \pi R/2$ where $\mathrm{d}s = R\, \mathrm{d}\theta$ is $t_{roll} \approx (a\eta/\lambda)R/E$. From arc length $s = 0$ to s_0 diffusion is faster than rolling. Unlike the unhooking time, the characteristic rolling time is not chain length-dependent. This chain length independent rolling is important in the formation of hooks about large circular obstacles: symmetric hooks form as chain halves roll to opposite sides of the obstacle. Likewise, release without hooking occurs using this rolling-off mechanism. Thus, in the strong field limit, both unhooking and rolling are important in the escape of polyelectrolyte chains impacted upon finite, circular obstacles.

These models account only for the potential-driven motion and ignore the random thermal forces which cause diffusive motion. Thermal motion is not important on the time scale of chain release whenever the obstacle is circular and the applied field is strong, $\beta N \gg 1$. This is evident from the magnitude of the distance, $\Delta = \sqrt{Dt}$, diffused by the chain during t_{unhook} and t_{roll}. During t_{unhook}, the distance diffused is on the order of a/β, which is considerably less than the downfield advance during unhooking, $Na/2$, for large chains and high fields. Likewise, the distance diffused during t_{roll} is R/β, which again is smaller than the downfield advance of R in large fields. Diffusion is however important at smaller time scales, for example, when the hook is formed with equal arms or when the initial impact occurs directly with charge/monomers distributed symmetrically over the obstacle. For circular obstacles and high fields, diffusion is not important on the collision time scale, even when the obstacle size is very large. One can see this by analysis of the center of mass trajectory on arc legnth s on a very large circular obstacle. We postulate that the chain advances diffusively from $s = 0$ to s_0 along the obstacle surface and undergoes field-induced rolling from s_0 until falloff. Between $s = 0$ and s_0, the rate of roll off is smaller than the rate of diffusion. Thus, the total collision time is comprised of the diffusion and the roll-off time with the s_0 demarcation being determined from minimization of the total collision time. The ratio of the diffusion time to roll-off time is $\approx \ln[a/(\beta NR)]^{1/2}$, indicating that diffusion is a small fraction of the collision time whenever the obstacle or field strength is large. Moreover, from this we also find that at field strengths $\beta N < a/R$ the collision time is dominated by diffusion. The simulation results presented in this paper are not at sufficiently low field strengths such that diffusion dominates the release mechanism.

IV. Collisions with a Large Obstacle

It is instructive to look first at a wide collection of chain collisions with a large obstacle, allowing for not only direct but also a range of indirect impacts, $b > 0$. We consider here the impact of a $N = 100$ chain in high field, $E = 20$, against an obstacle of radius $R = 60$ (with an inner hard core radius of $H = 40$), and dimensionless size, $\gamma = 15$. The average linear extent of the relaxed chain is $\langle l \rangle = 12.2$. Figure 4 provides the collision distance, z_c, versus collision time, t_c. The (z_c,t_c) data are banded, reflecting discrete sampling of the impact parameter from $b = 0$ (rightmost vertical band of points) to $b_{\max} = R + \langle l \rangle = 72.5$ (leftmost band). Direct impacts, small b, retard the chain's downfield progress, extending the collision time, while chains with an offset of b up to $72.5 = 1.21R$ at most glance the obstacle and travel downfield relatively unaffected by the obstacle. Such noninteracting chains have a center of mass velocity which is independent of chain length, v_0, as delineated by the displacement−time line in Figure 4.

The breadth of collision distances within each impact band in Figure 4 is due to (1) a distribution of chain dimensions, $\langle l \rangle$, at all impacts and (2) chain stretching which may occur as part of the collision process in direct or nearly direct impacts. The prescriptions for chain "release" and initial configuration are based upon the positioning of the most upfield and most downfield monomers and not upon the center of mass's downfield location. Consequently, the measured downfield advance

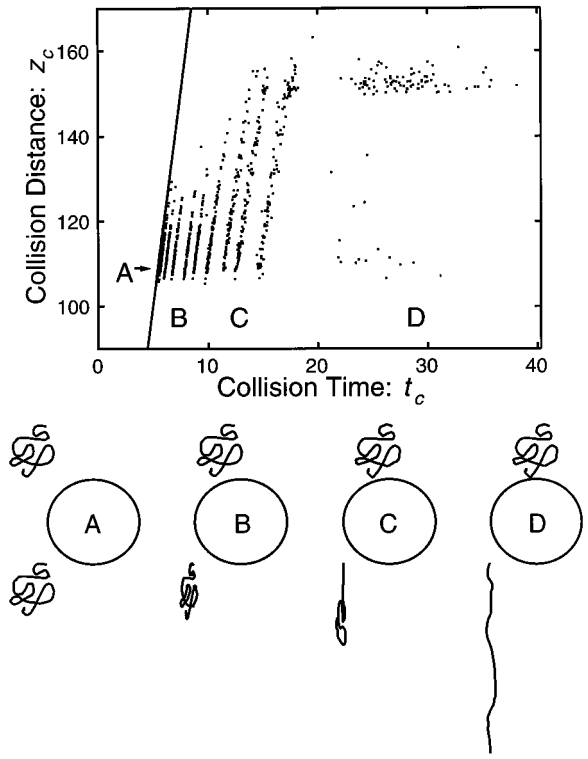

Figure 4. A plot of the collision distance, z_c, versus the collision time, t_c, for chains of $N = 100$ impacting upon an obstacle of radius $R = 60$ (dimensionless obstacle size $\gamma = 15$) with inner core radius of $H = 40$ and in high field, $E = 20$. Each of the 2400 points represents a simulated chain, and the banding of the data is due to the sampling of discrete offset of the chain's center of mass from the obstacle center. The offsets, quantified by the impact parameter b, are $b = 72.5$ to 60 (leftmost band), 40, 30, 20, 15, 10, 6, 4, 2, and 0 (rightmost band). These correspond to the full range of impacts $\langle l \rangle + R < b < 0$. Schematics of the chain at initial impact and final release is included for (A) no impact, (B, C) near glancing impacts, and (D) direct impact.

during collision, z_c, also reflects the distribution of chain extents, $\langle l \rangle$. This is evident on the most glancing impacts (schematic A in Figure 4), where the chain dimension is relatively unperturbed during the collision process. The average collision distance is $z_c = \langle l \rangle + R + H \approx 110$, with breadth in collision distance representing the distribution of chain extents. For more direct impacts the breadth of collision distances increases as chains are stretched during the collision. The maximum downfield advance occurs when the chain is fully stretched such that its center of mass is distance $Na/2$ downfield from the most upfield monomer; i.e., the maximum collision distance is $z_c \approx Na/2 + R + H + \langle l \rangle/2 = 150$ as shown in the schematic D of Figure 4. The collision distances sampled at direct ($b = 0$) impact are bimodal, indicating that upon release chains are either highly stretched or unperturbed. The highly stretched chains result from release through an unhooking mechanism while the unperturbed chains result from release through a simple rolling off of the obstacle.

We can explore the effect of obstacle size upon the collision distance and time at fixed field strength, $E = 20$. Figure 5 provides (z_c,t_c) results from the collision of chains of $N = 100$, 50, and 20 with a post of radii $R = 3$ (bottom) or $R = 60$ (top), corresponding to dimensionless obstacle sizes, γ, ranging from 0.74 to 33. The collision distances are larger for larger obstacles, indicative of the larger downfield advance which is needed to satisfy the rules of release. Focus first upon the data for the $N = 100$ chain (Figure 5a) impacted against obstacles of dimensionless size $\gamma = 0.74$ and for an intermediate-sized obstacle, $\gamma = 15$. Many of the chains impacted against the smaller obstacle are not dramatically impeded: their downfield advance occurs in times that are not very different from the downfield advance of a noninteracting chain, (i.e. the data points are close to the constant velocity, v_0, line of Figure 5a). However, if the chain is significantly "held up" by the obstacle, i.e., t_c is large, then the chain is highly stretched upon release, i.e., z_c is large. This shows that when the chain interacts significantly with the obstacle, release occurs predominantly by an unhooking mechanism and that nearly all chains that impact directly with the small

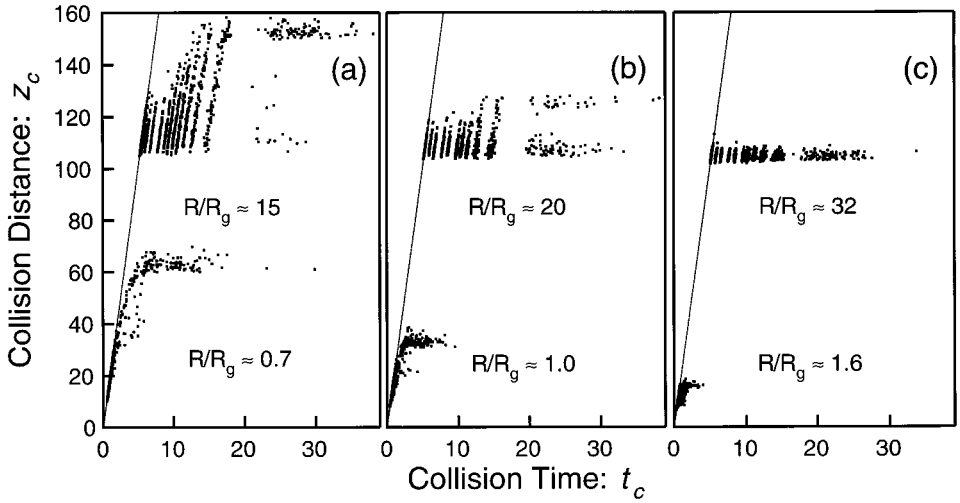

Figure 5. Plots of collision distance, z_c, versus collision time, t_c, for two different obstacles of radii $R = 3$ and $R = 60$ for chains of (a) $N = 100$, (b) $N = 50$, and (c) $N = 20$ monomers, with field strength $E = 20$ and over a range of impact parameters, $\langle l \rangle + R < b < 0$. Small obstacles, $\gamma < 1$, provide collision data that are similar to those of point posts; i.e., direct impacts result in hairpins which provide highly stretched chains upon release.[11] Chains impacted upon large obstacles, $\gamma \gg 1$, show data banding with impact parameter. There are two modes of release of chains impacted directly onto large posts: unhooking and "rolling off" of the obstacle. The unhooking mode is characterized by a long-lived chain interaction and strongly stretched chains upon release. The rolling-off mode is characterized by long-lived chain-obstacle interactions; however, the release conformation is unstretched and nearly relaxed. As the obstacle size increases, the proportion of hooked conformations diminishes until all chains are released through the rolling-off mode.

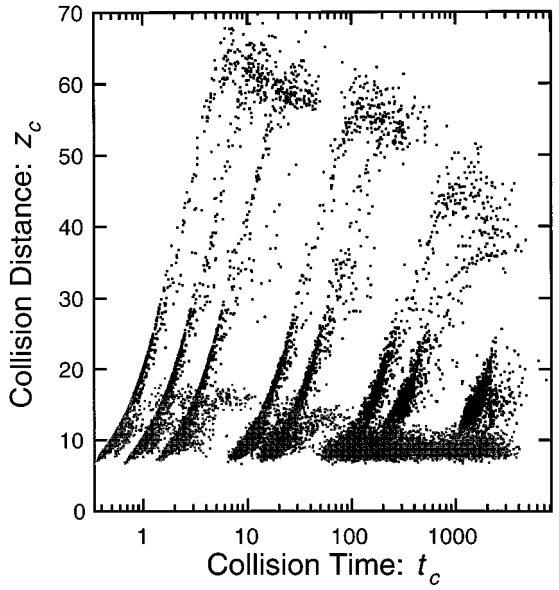

Figure 6. Semilogarithmic plots of collision distance, z_c, versus collision time, t_c, for chains of $N = 100$ (prominent "S"-shaped data bands) and $N = 20$ (low-lying data bands) impacted against an obstacle of radii $R = 3$ over a full range of impact parameters and at discrete field strengths $E = 20$ (leftmost band), 10, 5, 1, 0.5, 0.1, 0.05, and 0.01 (rightmost band). In high fields, distinguished by $NE\lambda a/k_BT \gg 1$, the data are characteristic of unhooking from an obstacle: there is an increase in collision distance with collision time and a plateau in the collision distance at larger collision times. However, when the field strength is low, the unhooking character is lost.

obstacle are released after long collision times. These results are very similar to previous results using a point obstacle and no thermal noise.[11] In contrast, more chains are held up by the larger obstacle, $\gamma = 15$, including those chains that indirectly impact with $b > 0$ (i.e., the data points are displaced significantly to the right of the constant velocity line in Figure 5). Moreover, these chains are not necessarily highly stretched upon release, indicating release by a rolling-off mechanism, with varying degrees of stretch. At direct impact, chain release also occurs after long collision times; however, the released chains can be unperturbed or highly stretched. As the obstacle increases in size, chains that impact directly are more likely to be released in an unperturbed conformation as opposed to a fully stretched conformation. This is particularly evident in the top of Figure 5a,b where the number of fully stretched chains (with $z_c \approx Na/2 + R + H + \langle l \rangle/2$) decreases while the number of unperturbed chains (with $z_c \approx \langle l \rangle + R + H$) increases at $b = 0$. In essence, chains that encounter obstacles that are large compared to the chain's natural dimensions will escape by a rolling-off mechanism. Hooks and unhooking are less likely to occur as the obstacle size increases.

V. An Ensemble of Collisions with Chains and Obstacles of Different Size

Figure 6 provides collision time and distances for $N = 100$ and $N = 20$ over a range of field strengths where collisions are explored over a full range of impacts with an obstacle of fixed radii $R = 3$ and dimensionless sizes $\gamma = 0.74$ and $\gamma = 1.6$. The $N = 100$ chains are in fields ranging from $\beta = 20$ to 0.01. The banding of data with impact parameter is not evident on these logarithmic scales; instead, the data are banded according to the applied field strength. As the field strength decreases, there is an increase in collision time, as one would expect from the decreased driving force. There is also a reduction in the maximum collision distance, signifying the diminished stretching of the arms of hooked chains in smaller applied fields. The signature of an unhooking mechanism is evident at all high field strengths: a rise in collision distance with collision time followed by a plateau in the collision distance at longer collision times. For the $N = 20$ chains, the obstacle size, while small, is on the order of the chain size, $\gamma = 1.6$, and the field strength ranges from $\beta = 20$ to $\beta = 0.01$. The $N = 20$ data are characteristic of the unhooking mechanism in strong fields, but this is lost when the field becomes weak. In weak field there is a characterless range of collision times and distances, with a loss of the plateau in collision distances. Thus, chains are not stretched in collision processes that occur at lower fields. Unhooking is not realized at weak fields simply because hairpins or hooks are not formed.

The universal scaling behavior found by Sevick and Williams for point obstacles shows that when chains impact a point obstacle, release occurs through an unhooking mechanism which follows simple scaling formulas.[11] Does the universal scaling behavior found for point posts in high field still hold for finite-sized posts and thermal motion? We can test this by measuring the degree to which the collision impedes the chains downfield advance in strong fields and by scaling with the same parameters as those used for point posts. In the simulations of Sevick and Williams, collision time and distance were measured only when the center of mass velocity was slower than v_0, i.e., when the chain was "slowed" by the post. Thus, it is first necessary to reduce a portion of the collision time and distance which result from unimpeded advance past a finite-sized obstacle. To recover zero collision distances in the finite post problem, the collision distance of a noninteracting chain, $\langle l \rangle + R + H$, is subtracted from all collision distances z_c. The time taken to traverse this distance in the absence of posts, $(\langle l \rangle + R + H)/v_0$, is subtracted from all collision times, t_c. This is done to recover zero collision time and distance for noninteracting chains. Finally, the collision time is scaled by the characteristic time for simple unhooking in a strong field, $t_{unhook} \approx E/N$, while the collision distance is scaled by the maximum extent of the chain, Na. All high field data with $\gamma = 0.74$ and 1.6 of Figure 6 were scaled in this fashion and result in Figure 7. Figure 7 shows that the universal behavior found for point posts with no thermal noise (see inset) is qualitatively reproduced for small, but finite-sized, obstacles with thermal noise. Noticeable in both is the long-lived state associated with hooked and fully stretched chains and the scaled constant velocity envelope, $v_0^* = dz^*/dt^* = \lambda/(2a^2\xi)$. Double-hooked hairpins which are distinguishable with point obstacles ($z_c^* = 0.25$) are also evident for finite-sized obstacles with thermal motion.

Similar treatment of the collision distance and time for large obstacles ($\gamma = 15$, 20, and 33) does not result in data collapse onto a single curve for various chain sizes and field strengths. This is expected as unhooking is no longer a dominant release mechanism. However, we can show that if we remove from the collision time the "slowing down" which results from the rolling-off mechanism, then we are able to see scaling behavior which is indicative of unhooking. To achieve this, we

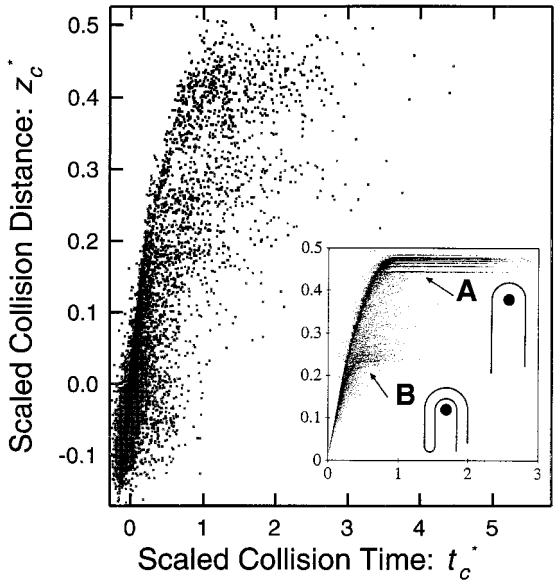

Figure 7. Scaled and reduced collision distance, z_c^*, versus scaled and reduced collision time, t_c^*, for chains of $N = 100$ and 20 at field strengths $E = 10$, 5, 1, 0.5, 0.1, and 0.05 and obstacle size $R = 3$, corresponding to small obstacles of dimensionless size $\gamma = 0.74$ and $\gamma = 1.6$. Each point in the graph represents one of the 13 800 collisions simulated. Collectively these points show that the collisions with small but finite obstacles scale similarly with noiseless ($k_BT = 0$) collisions on a point obstacle (inset).[11] Collisions with finite, but small, obstacles and with point obstacles gives rise to hooking (A) as well as multiple hooking (B), although thermal motion does give rise to some scatter in the points about the universal line.

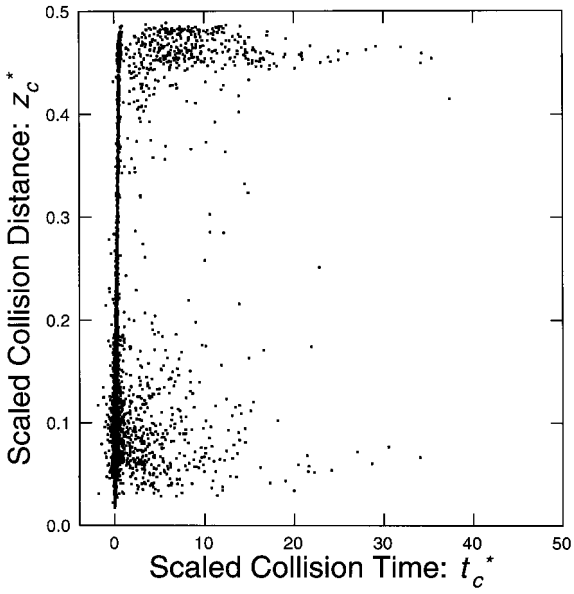

Figure 8. Scaled and reduced collision distance, z_c^*, versus scaled and reduced collision time, t_c^*, for chains of $N = 100$, 50, and 20 at field strengths $E = 20$ and 10 and obstacle sizes ranging from $R = 30$ to 120, corresponding to large obstacles of dimensionless size $7.4 < \gamma < 33$. These obstacles are large, and a significant fraction of the collision time will be dependent upon a chain size independent roll-off time which is dependent upon the impact parameter. The data reduction removes the effect of simple roll-off such that chains which are impeded by the obstacle are represented by points to the right of the constant velocity, v_o^*, line. Note that seriously impeded chains have scaled collision distances which span from $z_c^* = 0.5$, indicating that the chain is stretched out along the obstacle surface (possibly through hooking) toward $z_c^* = 0$, indicating near natural chain dimensions at release. This range of stretching occurs with the different dimensionless field strengths, βN, explored: larger dimensionless fields stretch the chain more while smaller fields do not significantly perturb chain dimensions.

must similarly reduce a portion of the collision time and distance which results not only from the unimpeded advance past the finite-sized obstacle but also from the rolling. Consider a chain that impacts the obstacle at impact parameter b and does not form a hook, but rolls off. This chain's measured collision time consists of a collision time that is in three parts. The first is the time that it takes for the center of mass to advance from $z = -(R + \langle l \rangle/2)$ until impact at $z = -b \sin \theta_0$ or $s = s_0$ and occurs at unimpeded velocity v_0. From θ_0 to $\theta = \pi/2$, the chain rolls off of the obstacle taking time $a\eta/\lambda(R/E)$ $\ln(\sin \theta_0/(1 - \cos \theta_0))$: this is the second component of the collision time. And the final time portion occurs during center of mass transit between from $z = 0$ ($\theta = \pi/2$) to $z = H + \langle l \rangle$, where the most upfield monomer is at $z = H$ meeting the condition of release, at a velocity v_0. This discount time depends upon the chain's impact parameter b and is subtracted from each t_c measurement. Similarly, the finite size of the obstacle is subtracted from each collision distance z_c to remove the obstacle-size-dependent part of the chain's center of mass advance. These discounted times and distances are then scaled according to the characteristic time and length scales of unhooking, i.e., t_{unhook} and Na, respectively. The result is Figure 8, and it is very similar to the scaled time/collision behavior of point posts, with the exception that most chains are not significantly retarded by hooking; i.e., most of the points lie on a constant velocity, v_0^*, line. Those chains that are seriously impeded possess a range of collision distances, indicating the chains range from fully stretched to completely unperturbed at release. All field strengths explored were $\beta N > a/R$ such that diffusion did not dominate the release time.

VI. Conclusions

In this paper we have used a Brownian dynamics simulation to study the field-driven collision of a polymer chain with a circular, ionically conductive obstacle of radius R described by a dimensionless size $\gamma = R/(a\sqrt{N/6})$. We have demonstrated that there are two separable, field-driven modes of release from circular obstacles with dimensionless field strengths $\beta N > a/R$. The first is the unhooking mode of release which occurs on a chain-length-dependent time scale, $t_{unhook} = a\eta/\lambda(N/E)$. It was shown that the release mechanism mode permits the universal scaling of collision time over a range of strong field strengths and chain sizes for collisions with point posts. In this paper, where we have included thermal motion and considered finite obstacles, we find that this universal scaling behavior is retained, particularly for small obstacles. When the obstacle is increased in size, $\gamma > 1$, a second mode of release becomes more likely than the unhooking mode. This second mode consists of the chain rolling off of the obstacle on a time scale $t_{roll} = (a\eta/\lambda)R/E$, which is independent of chain length but dependent upon the obstacle size and the type of collision, that is, whether it is direct or glancing impact. As such, stochastic collisions with large obstacles do not segregate the chains according to size, but rather impart a distribution to the downfield advance which reflects the size of the obstacles. While important at small time scales, diffu-

sion does not occur on the time scale of the release kinetics when the obstacle is circular, regardless of the large size of the obstacle and when the field is $\beta N > a/R$. Diffusion is important on the collision time scale only for completely flat obstacles, as for example, perforated barriers. Our study of chain−obstacle collisions is currently being extended to the case of nonconductive obstacles which distort the local electric field.

Acknowledgment. The authors thank The Australian National University Supercomputer Facility (ANUSF) for an allocation of computation time on a Silicon Graphics Power Challenge XL.

References and Notes

(1) Doi, M.; Edwards, S. F. *The Theory of Polymer Dynamics*; Oxford University Press: Oxford, 1986.
(2) Giurrieri, S.; Rizzarelli, E.; Beach, D.; Bustamante, C. *Biochemistry* **1990**, *29*, 3396.
(3) Perkins, T. T.; Quake, S. R.; Smith, D. E.; Chu, S. *Science* **1994**, *264*, 822.
(4) Perkins, T. T.; Quake, S. R.; Smith, D. E.; Chu, S. *Science* **1997**, *276*, 2016.
(5) Volkmuth, W. D.; Austin, R. H. *Nature* **1992**, *358*, 600.
(6) Volkmuth W. D.; Duke, T.; Wu, M. C.; Austin, R. H. *Phys. Rev. Lett.* **1994**, *72*, 2117.
(7) Duke, T.; Monnelly, G.; Austin, R. H.; Cox, E. C. *Electrophoresis* **1997**, *18*, 17.
(8) Song, L.; Maestre, M. F. *J. Biomol. Struct. Dyn.* **1991**, *9*, 87.
(9) Deutsch, J. M.; Madden, T. L. *J. Chem. Phys.* **1989**, *90*, 2476.
(10) Burlatsky, S.; Deutch, J. *Science* **1989**, *260*, 2476. Viovy, J. L.; Duke, T. *Science* **1994**, *246*, 112.
(11) Sevick, E. M.; Williams, D. R. M. *Phys. Rev. Lett.* **1996**, *76*, 2595.
(12) Nixon, G. I.; Slater, G. W. *Phys Rev. E* **1994**, *50*, 5033.
(13) Sevick, E. M.; Williams, D. R. M. *Phys. Rev. E* **1994**, *50*, R3357.
(14) Masubuchi, Y.; Oana, H., Akiyama, T.; Matsumoto, M.; Doi, M. *J. Phys. Soc. Jpn.* **1995**, 1412.
(15) Oana, H., Akiyama, T.; Matsumoto, M.; Doi, M. *Macromolecules* **1994**, *27*, 6061.
(16) Manning, G. S. *J. Phys. Chem.* **1981**, *85*, 1506.
(17) Long, D.; Viovy, J.-L.; Adjari, A. *Phys. Rev. Lett.* **1996**, *76*, 3858.
(18) Andre, P.; Long, D., Adjari, A. *Eur. Phys. J. B* **1998**, *4*, 307.

MA981049G